

## Article

# Cobalt Nanoparticle-Embedded Nitrogen-Doped Carbon Catalyst Derived from a Solid-State Metal-Organic Framework Complex for OER and HER Electrocatalysis

Shaik Gouse Peera <sup>1,\*</sup>, Ravindranadh Koutavarapu <sup>2</sup>, Chao Liu <sup>3</sup>, Gaddam Rajeshkhanna <sup>4,\*</sup>, Arunchander Asokan <sup>5,\*</sup> and Ch. Venkata Reddy <sup>2,\*</sup>

<sup>1</sup> Department of Environmental Science, Keimyung University, 1095 Dalgubeol-daero, Dalseo-gu, Daegu 42601, Korea

<sup>2</sup> School of Mechanical Engineering, Yeungnam University, Gyeongsan 712-749, Korea; ravindra.physicist@gmail.com

<sup>3</sup> Engineering Research Center for Hydrogen Energy Materials and Devices, Faculty of Materials Metallurgy and Chemistry, Jiangxi University of Science and Technology, Ganzhou 341000, China; liuchao198967@126.com

<sup>4</sup> Department of Chemistry, National Institute of Technology Warangal, Warangal 506004, Telangana, India

<sup>5</sup> Faculty of Mechanical Engineering, Technion-Israel Institute of Technology, Haifa 32000, Israel

\* Correspondence: gouse@kmu.ac.kr (S.G.P.); grkhanna@nitw.ac.in (G.R.); a.asokan@campus.technion.ac.il (A.A.); cvrphy@gmail.com (C.V.R.)



**Citation:** Peera, S.G.; Koutavarapu, R.; Liu, C.; Rajeshkhanna, G.; Asokan, A.; Reddy, C.V. Cobalt Nanoparticle-Embedded Nitrogen-Doped Carbon Catalyst Derived from a Solid-State Metal-Organic Framework Complex for OER and HER Electrocatalysis. *Energies* **2021**, *14*, 1320. <https://doi.org/10.3390/en14051320>

Academic Editor: Adriano Sacco

Received: 26 January 2021

Accepted: 22 February 2021

Published: 1 March 2021

**Publisher's Note:** MDPI stays neutral with regard to jurisdictional claims in published maps and institutional affiliations.



**Copyright:** © 2021 by the authors. Licensee MDPI, Basel, Switzerland. This article is an open access article distributed under the terms and conditions of the Creative Commons Attribution (CC BY) license (<https://creativecommons.org/licenses/by/4.0/>).

**Abstract:** Electrochemical water splitting is considered a promising way of producing hydrogen and oxygen for various electrochemical energy devices. An efficient single, bi-functional electrocatalyst that can perform hydrogen evolution reactions (HERs) and oxygen evolution reactions (OERs) is highly essential. In this work, Co@NC core-shell nanoparticles were synthesized via a simple, eco-friendly, solid-state synthesis process, using cobalt nitrate and with pyrazole as the N and C source. The morphological analysis of the resulting Co@NC nanoparticles was performed with a scanning and transmission electron microscope, which showed Co nanoparticles as the core and the pyrolysis of pyrazole organic ligand N-doped carbon derived shell structure. The unique Co@NC nanostructures had excellent redox sites for electrocatalysis, wherein the N-doped carbon shell exhibited superior electronic conductivity in the Co@NC catalyst. The resulting Co@NC nanocatalyst showed considerable HER and OER activity in an alkaline medium. The Co@NC catalyst exhibited HERs overpotentials of 243 and 170 mV at 10 mA·cm<sup>-2</sup> on glassy carbon and Ni foam electrodes, respectively, whereas OERs were exhibited overpotentials of 450 and 452 mV at a current density of 10 and 50 mA·cm<sup>-2</sup> on glassy carbon electrode and Ni foam, respectively. Moreover, the Co@NC catalyst also showed admirable durability for OERs in an alkaline medium.

**Keywords:** water splitting; cobalt catalyst; hydrogen evolution reaction; oxygen evolution reaction

## 1. Introduction

The increased global energy demand due to the increasing population escalates the use of greenhouse gas emitting fossil fuels, which has researchers searching for alternative, efficient, sustainable, and less carbon emission-free technologies. In this regard, electrochemical water splitting is considered a promising technology for obtaining hydrogen for energy-producing technology like hydrogen-based fuel cells and regenerative fuel cells [1]. The hydrogen evolution reaction (HER) and oxygen evolution reaction (OER), during the electrolysis process, occurs at a cathode and anode, respectively. Both reactions require highly active electrocatalysts such as Pt-based catalysts for cathodes and Ir/Ru-based catalysts for anodes. Water electrolysis can be performed in acidic or basic electrolytes. Although acidic-based water electrolysis systems are widespread, they are limited, hindering

the market penetration due to the utilization of expensive Pt and Ir/Ru-based electrocatalysts [2]. On the other hand, alkaline water electrolysis is considered a promising way of reducing the overall cost of the electrolysis device, as it allows to use of cost-effective, earth-abundant transition metals as electrocatalysts for electrode reactions.

In view of this, considerable efforts have been made to develop efficient and cost-effective electrocatalysts from 3D transition metals such as Fe, Ni, Co, Mn, etc. [3–5]. Among all the transition metals, Co has emerged as attractive for electrochemical water splitting due to its rich redox chemistry and superior catalytic performance [6]. Accordingly, several researchers synthesized a variety of Co-based catalysts such as cobalt-chalcogenides, Co-catalysts derived from layered double hydroxide, and metal-organic frameworks [7,8]. Furthermore, Co-catalysts supported on porous, conductive, high surface area catalytic carbons were found to be an effective strategy for better exposure of the metal centers for rich redox reactions during the HER and OER processes, thus enhancing overall performance and electrocatalytic activity. A variety of conductive carbons such as Vulcan carbons, N-doped carbon nanotubes (CNTs), graphene, etc., have been utilized [9]. Recently, carbon-encapsulated metal nanoparticles (metal@carbon) have attracted considerable attention due to their enhanced stability arising from the thick carbon layers around the Co nanoparticles and their stability over a wide pH range [10]. In addition, the encapsulated carbon shells have been found to greatly avoid Co nanoparticle aggregation, resulting in excellent long-term stability. Furthermore, it has been found that the doping of heteroatoms such as N (metal@N-carbon) into the carbon shells can give rise to unique electronic properties in the metal@NC nanoparticles due to their synergistic role in effective electron transfer between N-doped carbon shells and metal nanoparticles during OER and HER reactions. In this regard, a variety of M@NC (M=Fe, Co, Mn, Ni, etc.) catalysts have also been synthesized [3–5].

Electrocatalysts derived from metal-organic frameworks (MOFs) have received a great deal of attention in recent times for use in various electrochemical reactions such as the oxygen reduction reaction (ORR), OER, and HER [11,12]. MOFs are a class of porous materials made of metal ions and organic ligands that can be structured in one, two, and three-dimensional arrays. MOFs of various sizes, shapes, pore geometry can be synthesized by different metals and a wide variety of organic ligands. Furthermore, by using organic ligands consisting of heteroatoms such as N, S, etc., MOFs can be synthesized by selecting a specific pyrolysis temperature. A variety of synthetic protocols, such as solvothermal, hydrothermal, sono-chemical, microwave synthesis methods, have been adopted to synthesize MOF-derived catalysts [13]. However, synthesis of MOFs is generally performed in the presence of organic solvents such as dimethylacetamide, triethylamine, ethanol, methanol, N-methyl formamide, etc., which possess a continuous threat to the environment. Recently, it has been advised by EU REACH regulations (the EU regulations on registration, evaluation, authorization, and restriction of chemicals), promoting concerns about the use of organic solvents for various chemical reactions [14]. Many of the organic solvents generally used in chemical laboratories for the synthesis of various materials pose a severe threat due to their reproductive toxicity. It is likely that supplies of solvents such as dimethylformamide, N-methylpyrrolidone, and dimethylacetamide, etc., may be restricted under the EU REACH regulations soon. Hence, it is of paramount importance to shift the chemical synthesis protocols to the use of greener solvents or complete elimination of solvents during reaction steps; research into greener solvents is highly encouraging.

Solvent-free-mechanochemical synthesis protocols have been recently receiving great interest as the problems regarding the use of organic solvents can be eliminated. Mechanochemical synthesis involves simple mixing of the reagents in a motor and pestle by a simple mechanical grinding or by a specially designed reactor. Further, mechanochemical synthesis has great potential to scale up the reaction parameters to pilot scale. Recently, we have synthesized Co@NC nanoparticles from a solid-state, mechanochemical synthesis protocol with Zn and Co as metal atoms and pyrazole as the organic ligand (source of C and N). The successful MOF-like self-assembly of Zn and pyrazole ligand to  $Zn_xCo_{1-x}(C_3H_4N_2)$  MOFs

was proven, and the pyrolysis of the  $Zn_xCo_{1-x}(C_3H_4N_2)$  resulted in Co encapsulated by N-doped carbon (Co@NC). The Co@NC catalyst was tested for electrocatalytic activity for ORR in both acidic and alkaline electrolytes, which showed admirable activity and durability [15]. In this work, we have tested the ability of the Co@NC nanoparticles in the context of HER and OER activity.

## 2. Materials and Methods

### 2.1. Synthesis of the Co@NC Catalysts

All the chemicals and reagents were used as received without any further purifications. The Co@NC catalyst was synthesized in a similar way as reported in our previous work [15]. Briefly, a calculated amount of Zinc acetate ( $Zn(OAc)_2$ ), pyrazole, cobalt nitrate precursors were placed into a mortar and mechanically ground uniformly with a pestle for about 30 min and left the material to room temperature until it dried. This led to the formation of the precursor,  $Zn_xCo_{1-x}(C_3H_4N_2)$ . The dried mixture was subjected to the direct pyrolysis in an inert atmosphere in a tubular furnace at 950 °C for about 1 h, with a heating rate of 5 °C min<sup>-1</sup>, under a N<sub>2</sub> atmosphere. After pyrolysis, the Co@NC catalyst was collected and finely ground, and used for physical and electrochemical characterizations. No solvent was utilized anywhere in the entire synthesis process. In a second process, the  $Zn_xCo_{1-x}(C_3H_4N_2)$  mixture was applied manually onto the pre-cleaned Ni foam directly while wet and allowed the Ni foam (1 × 1 cm<sup>-2</sup>) to dry. The dried Ni foam was further subjected to pyrolysis in the tubular furnace at 950 °C for about 1 h, with a heating rate of 5 °C min<sup>-1</sup>, under a N<sub>2</sub> atmosphere. After the pyrolysis, the Co@NC catalyst was deposited on the Ni foam (Co@NC/Ni foam) and was used for electrochemical studies.

### 2.2. Physical and Electrochemical Characterizations

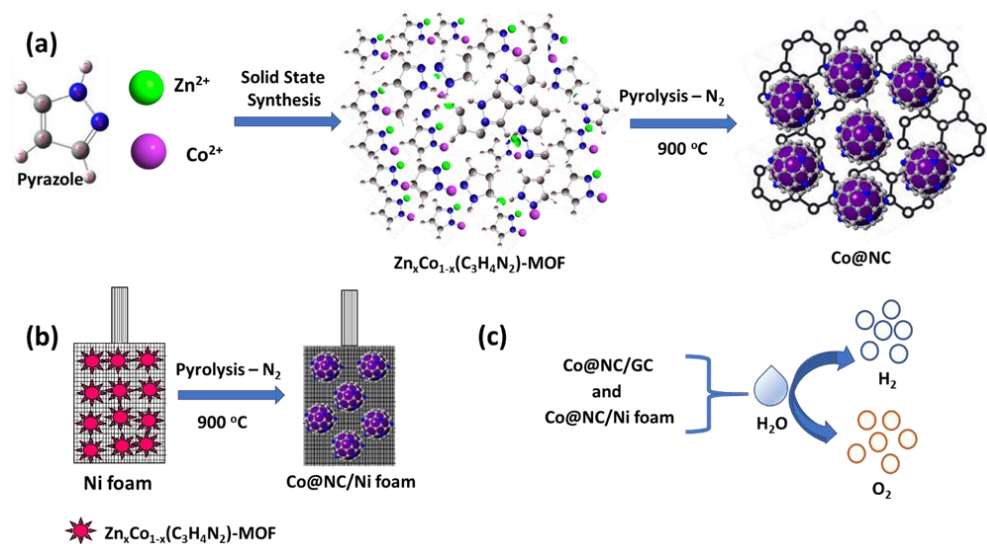
Morphological characterization of the synthesized catalysts was performed by using a scanning and transmission electron microscope (FEI QUANTA FEG 650). X-ray diffraction analysis of the catalyst was performed using a PAN analytical X-ray diffractometer at 1.54 Å CuK $\alpha$  radiation. X-ray photoelectron spectroscopy (XPS) of the catalysts was obtained using a Thermo Fisher Scientific, ESCALAB 250 XPS system.

Electrochemical characterizations of the catalysts were performed in a 1.0 M KOH electrolyte with a VSP/VMP 3B-20, potentiostat/galvanostat provided by Biologic instruments Inc. All the characterizations were performed in a three-electrode system in which catalyst ink was deposited on to glassy carbon electrode (GCE, geometric area: 0.071 cm<sup>2</sup>) or pre-treated Ni foam (1 × 1 cm<sup>2</sup>) as the working electrode, Ag/AgCl (sat. KCl) as the reference electrode and Pt wire as the counter electrode. The catalyst ink was prepared by dispersing a calculated amount of Co@NC/RuO<sub>2</sub>/Pt/C catalysts in a mixed solution of isopropyl alcohol, water, and Nafion binder and ultrasonicated for 30 min. The catalyst ink was deposited by a drop-casting method onto GCE and allowed to dry under ambient conditions. In the second process, a mixture of isopropyl alcohol and Nafion (5 wt.%) binder was dropped on the Co@NC/Ni foam and allowed to dry at room temperature. In both the processes, the final catalyst loading was maintained at ~1 mg·cm<sup>-2</sup> on GCE and ~2 mg·cm<sup>-2</sup> on Ni foam. All potentials were converted to the reversible hydrogen electrode (RHE) scale for convenience unless otherwise specifically stated ( $E_{RHE} = E_{Ag/AgCl} + 0.059 \times pH$ ). All the electrochemical characterizations were performed using the 1.0 M KOH electrolyte.

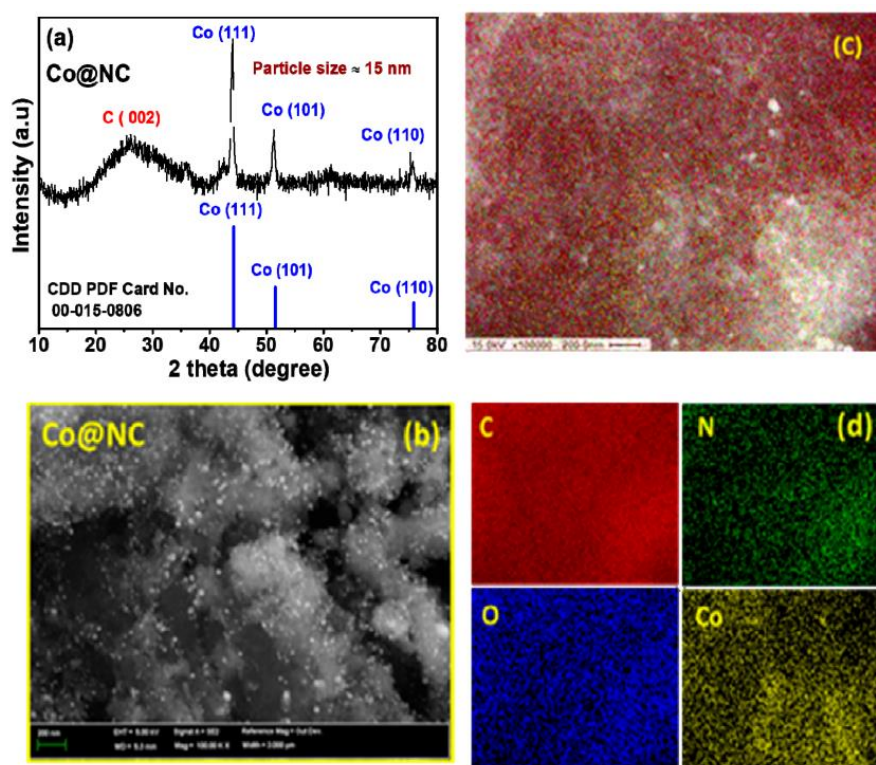
## 3. Results

Figure 1a shows the pictorial representation of the synthesis of Co@NC nanoparticles by a solid-state mechanochemical synthesis process. A calculated amount of the precursors were taken (Co<sup>2+</sup>, pyrazole, and Zn<sup>2+</sup>) together into a mortar and mechanically ground with a pestle for about 30 min, which leads to the formation of a sticky pink-colored paste, which upon drying produced a solid pink colored powder. As in our proposed mechanism for forming self-assembled MOF structures in our previous work [15], during the

mechanical grinding process, the mechanical force allowed the formation of coordination bonds between -N groups of the pyrazole ligand with Zn, and -NH pyrazole with  $\text{Co}^{2+}$  ions, finally forming a self-assembled  $\text{Zn}_x\text{Co}_{1-x}(\text{C}_3\text{H}_4\text{N}_2)$  MOF structure. The resulted  $\text{Zn}_x\text{Co}_{1-x}(\text{C}_3\text{H}_4\text{N}_2)$  MOF structures were further subjected to pyrolysis under an inert atmosphere. During the pyrolysis process, the pyrazole ligands carbonized into N-doped carbon shells,  $\text{Co}^{2+}$  coordinated with pyrazole ligands underwent carbo-reduction to metallic Co nanoparticles, whereas metallic Zn atoms evaporated and were taken out via the gas stream (boiling point of metallic Zn is  $908^\circ\text{C}$ ). The possible formation of  $\text{Zn}_x\text{Co}_{1-x}(\text{C}_3\text{H}_4\text{N}_2)$  MOF structures was identified by the contrasting diffraction patterns for the add-mixture of  $\text{Zn}_x\text{Co}_{1-x}(\text{C}_3\text{H}_4\text{N}_2)$  when compared to all other precursor's diffraction patterns, as described in our previous work [15]. In a second synthesis step (Figure 1b), the self-assembled  $\text{Zn}_x\text{Co}_{1-x}(\text{C}_3\text{H}_4\text{N}_2)$  precursor (in wet conditions) obtained right after mechanical grinding was directly applied to the pre-cleaned Ni foam uniformly and left to dry at room temperature. After drying, the Ni foam was subjected to pyrolysis at  $950^\circ\text{C}$ . We hypothesized that by the similar mechanism discussed above, Co@NC nanostructures would form when directly deposited onto the Ni foam. Figure 2a shows the diffraction patterns of the Co@NC catalyst obtained after pyrolysis, which show the diffraction peaks at  $25.9^\circ$ ,  $44^\circ$ ,  $51^\circ$ , and  $75^\circ$ , which were attributed to C (002), Co (111), Co (101), and Co (110). The reflections in the X-ray diffraction (XRD) patterns were indexed based on the crystalline cubic system of cobalt (International center for diffraction data - powder diffraction file (ICDD-PDF Card No. 00-015-0806)). The crystal size of the Co (111) particles was calculated using the Scherrer equation from the diffraction data and was found to have an average value of  $\sim 15$  nm. The morphological observation of the Co@NC catalyst was performed by SEM and TEM measurements. Figure 2b shows the SEM images of the Co@NC catalyst. From the SEM images, it can be clearly observed that the nanosized Co nanoparticles were evenly distributed on the surface of N-doped carbon support derived from the carbonization of the pyrazole ligand. Furthermore, the mapping of a selected area showed the presence of dense elements of C, N, O, and Co, as shown in Figure 2c,d.



**Figure 1.** (a) Schematic representation of the synthesis of Co@NC catalyst by a mechanochemical synthesis process (b) synthesis of Co@NC catalyst on Ni foam (c) application of Co@NC catalyst for water splitting.



**Figure 2.** (a) X-ray diffraction patterns of Co@NC catalyst. (b) SEM images of Co@NC catalysts. Corresponding quantitative energy dispersive X-ray spectroscopy (EDS) elemental mapping of C, O, N and Co (c) combined map (d) individual mapping of elements.

TEM images (Figure 3) of Co@NC catalyst show the Co nanoparticles of nanometer range were deposited on the N-doped carbon support. A closer look at the images further revealed clear Co@NC core-shell structures, in which N-doped carbon wraps around the Co nanoparticles. The d-spacing of the lattice fringes of metallic Co nanoparticle was identified as being 0.209 nm, corresponding to the Co (111) plane (Figure 3e, inset). Furthermore, the Co nanoparticles particle size measured using TEM images, the corresponding histogram, and distribution curve shows, Co@NC catalyst exhibited an average particle size ranging from 10–12 nm (Figure 3f, inset). During pyrolysis, the carbonization of the pyrazole ligand to N-doped carbon shells took place together with the carbo-reduction of  $\text{Co}^{2+}$  ions to metallic Co atoms, in parallel to the evaporation of Zn species. Because the mass of the pyrazole ligand was higher than the  $\text{Co}^{2+}$ , the  $\text{Co}^{2+}$  ions are spatially isolated from each other, and the presence of Zn atoms further ensured this special distance in the  $\text{Zn}_x\text{Co}_{1-x}(\text{C}_3\text{H}_4\text{N}_2)$  MOF structures. Due to this definite distribution, the aggregation of Co nanoparticles during the pyrolysis process was mitigated [16]. Furthermore, the continuous carbonation of the pyrazole ligand to N-doped carbon also acted as a protective covering around the Co metal nanoparticles. All these phenomena led to the formation of definite Co@NC core-shell nanostructures. The metallic evaporation of Zn species during pyrolysis led to the porous structure of the N-doped carbon. The Brunauer–Emmett–Teller (BET) surface area of the Co@NC nanostructures was found to  $371 \text{ m}^2 \text{ g}^{-1}$ , along with the presence of mesopores in a 4–6 nm range (measured in our previous studies [15]). The presence of mesopores ensured the enhanced transfer of reactants towards the active catalytic sites and the desorption of the products away from the catalytic sites.

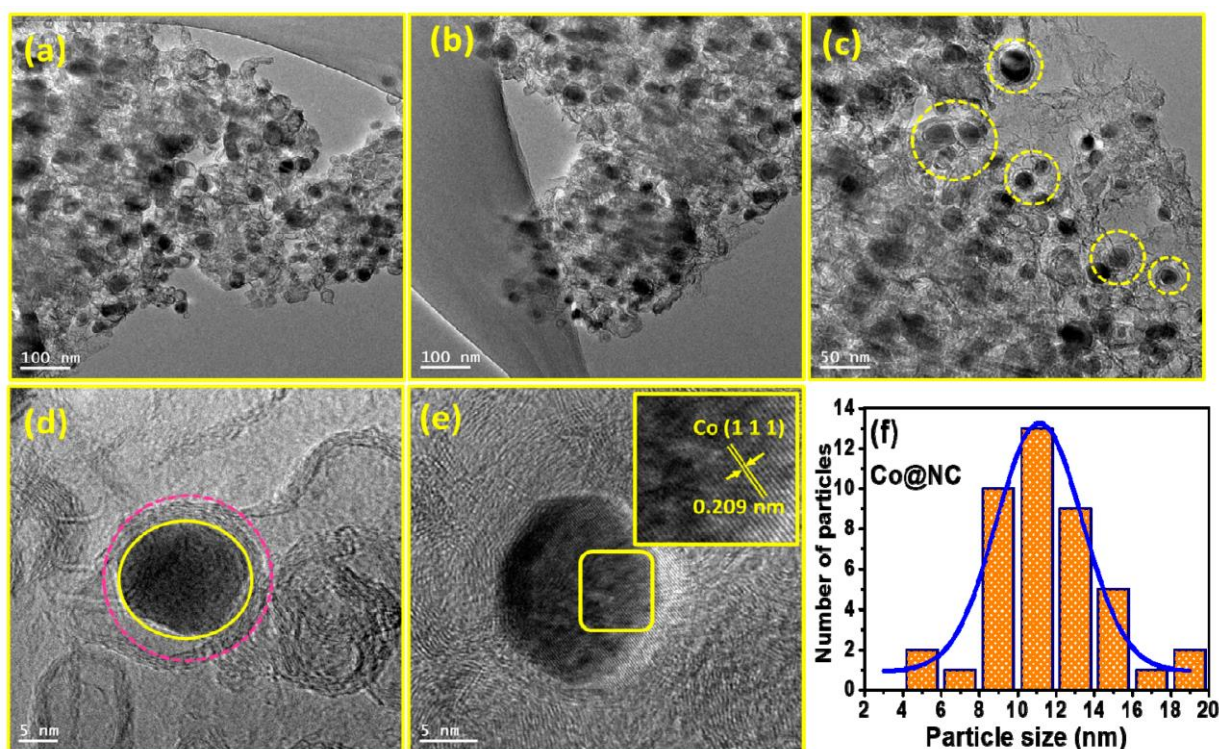


**Figure 3.** TEM images (a–e) of Co@NC nanostructures (f) histogram of particle size and statistical distribution curve of Co nanoparticles derived from TEM images.

XPS analysis was performed to identify the chemical composition of the electrocatalyst. Figure 4a shows the XPS survey spectrum of the Co@NC catalyst. The survey scan showed the presence of C, N, O, and Co in the catalyst. Furthermore, high-resolution scanning was performed to identify the chemical states of each element in the catalyst. All the high-resolution scanning data were deconvoluted into individual peaks corresponding to individual chemical states of the elements. Figure 4b shows the C1s spectra deconvoluted into four peaks corresponding to  $\text{—C—C}$ ,  $\text{C—N}$ ,  $\text{—C=O}$ , and  $\text{—O—C=O}$  chemical states of carbon at binding energies of 284.2, 284.9, 286.4, and 289.0 eV, respectively. The deconvoluted C1s spectra infer the presence of C, N, and O in the Co@NC catalysts; the presence of  $\text{C—N}$  especially demonstrates the successful doping of N into the carbon matrix of Co@NC catalyst. Figure 4c shows the deconvoluted N1s spectra, which revealed that the doped N in the carbon matrix existed in three different forms, which were pyridinic-N, pyrrolic-N, and graphitic-N at the binding energies of 397.3, 399.8, 401.1 eV, respectively, which further confirms the presence and successful doping of the N into the carbon matrix. Both theoretical and experimental studies demonstrate that all these forms contribute to the electrocatalytic activity of carbons in different proportions. Especially, graphitic-N and pyridinic-N are known to play important roles in enhancing the electronic conductivity of the catalyst through induced spin density and charge distribution on the carbon  $\pi$  conjugation system [17]. And graphitic-N and pyridinic-N are also known as the major catalytic sites with the lowest barrier for the rate-determining first electron transfer step, in addition to their selectively in promoting a dominant 4 electron  $\text{O}_2$  electrode pathway [18]. Pyridinic-N and graphitic-N share their lone pair of electrons with the carbon shell, which increases the electronic density around the Co nanoparticles by decreasing the work function of Co nanoparticles towards the OER and HER [19]. N1s spectra also showed a peak associated with the possible atomic Co coordinated with the pyridinic-N, which are popularly called  $\text{M—N}_x\text{—C}$  or  $\text{Co—N}_x\text{—C}$  moieties, the existence of which was confirmed in many  $\text{M—N}_x\text{—C}$  catalyst systems by advanced characterization techniques [20]. These special  $\text{M—N}_x\text{—C}$  are known to enhance the OER and HER kinetics via enhanced charge transfer from the N—C shell to the Co atoms [21]. Figure 4d shows the  $\text{Co } 2_p^{3/2}$  spec-

tra, separated into three deconvoluted peaks at 778.7, 779.7, and 781.4 eV, which were attributed to the metallic Co, Co—N<sub>x</sub>—C, and CoN<sub>x</sub>, respectively. Co spectra also showed a broad satellite peak at the binding energies of ~800 eV, which revealed the presence of antibonding orbitals between Co and possible oxygen moieties. The presence of a satellite peak suggested that the electronic configuration of Co was close to  $t_{2g}^6 e_g^1$ , which is near the optimal  $e_g$  filling, and hence effectively promotes the breaking of M—OH— bond, therefore favoring high electrocatalytic activity towards oxygen catalysis [22]. It was also demonstrated by the density functional theory (DFT) calculations that Co—N—C structure plays a key role in HER activity, while the Co active-sites play a role in OER activity [23].

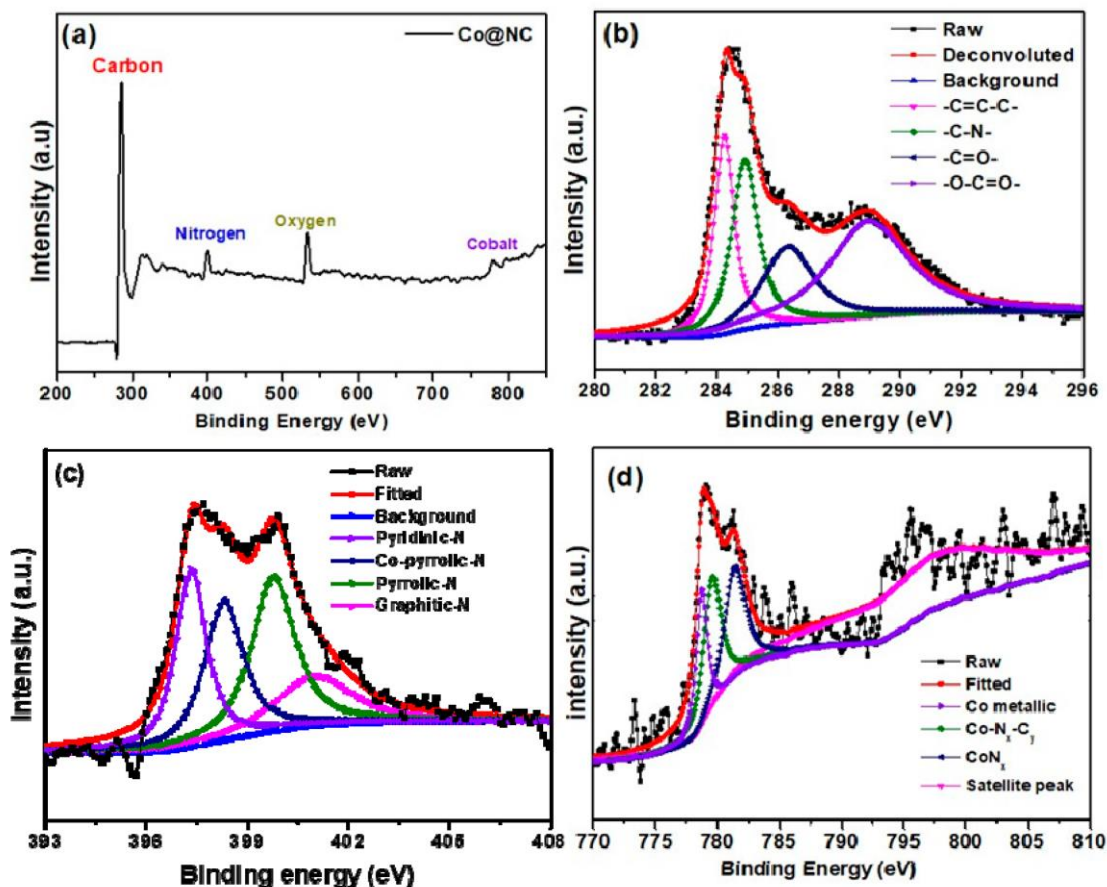


**Figure 4.** (a) X-ray photoelectron spectroscopy (XPS) survey spectra of the Co@NC catalyst and high-resolution deconvoluted spectra of the (b) C1s, (c) N1s, and (d) Co 2p spectra.

The bifunctional OER and HER analysis of the Co@NC catalyst were studied in a 1.0 M KOH electrolyte solution. Figure 5a shows the HER linear sweep voltammetry (LSV) polarization curves of bare GCE, Co@NC catalyst, and Pt/C (20 wt.%). Indeed the Pt/C catalyst showed excellent HER activity, very close to the thermodynamic HER potential of the Pt electrode. When compared to bare glassy carbon (GC), which almost had no considerable HER activity, the deposited Co@NC catalyst showed appreciable HER activity. An overpotential of 243 and 59 mV was observed at a current density of  $10 \text{ mA}\cdot\text{cm}^{-2}$  for Co@NC and Pt/C catalysts, respectively. The Co@NC catalyst was 184 mV away from the benchmark Pt/C catalyst. Further, the Tafel analysis revealed that the GC, Co@NC, and Pt/C catalysts showed a Tafel slope of 409, 101, and  $61 \text{ mV}\cdot\text{dec}^{-1}$ , respectively (Figure 5b). The Co@NC catalyst's Tafel slope was lesser than the bare GC's, which confirmed HER activity arose from the Co@NC catalyst. For practical applications evaluating electrode material activity on the large area of a current collector such as Ni foam is essential.

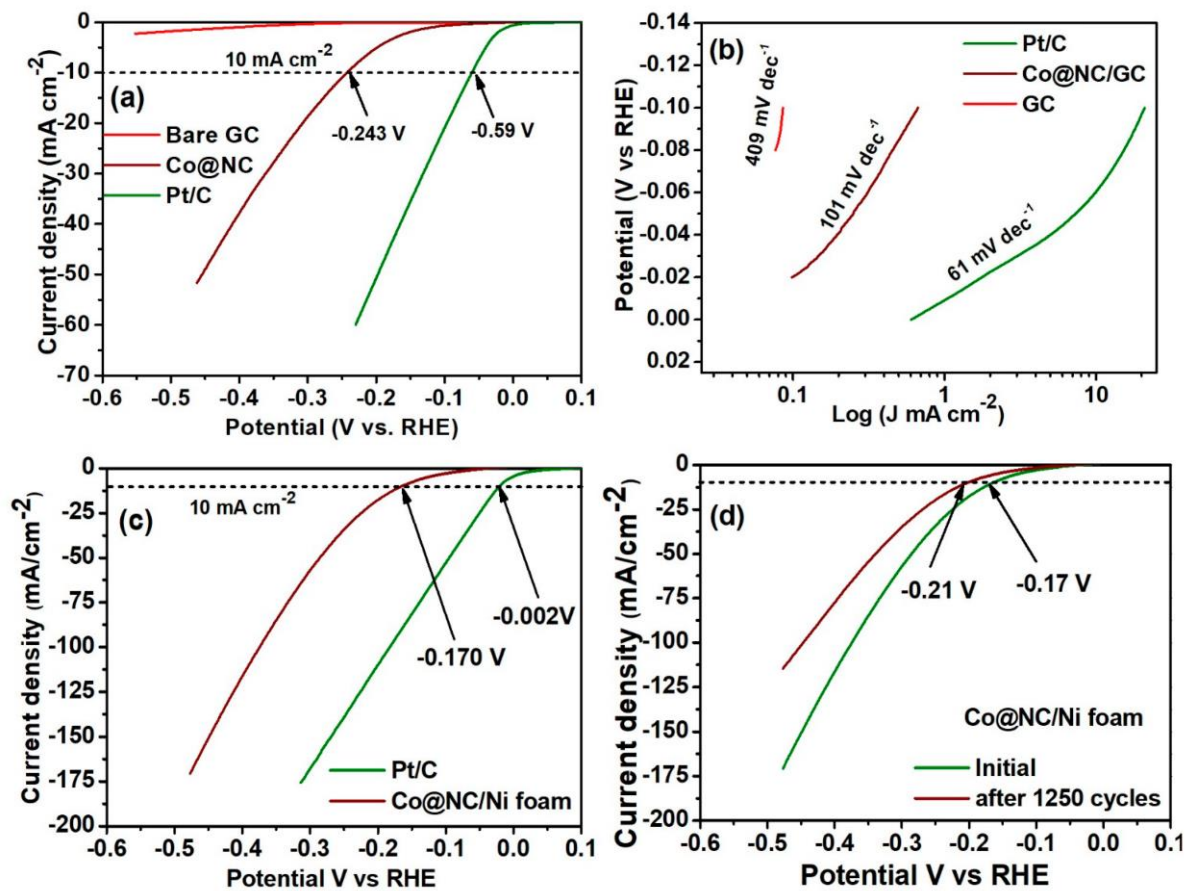


**Figure 5.** Hydrogen evolution reaction (HER) LSVs measured at  $5 \text{ mV}\cdot\text{s}^{-1}$  in  $1.0 \text{ M KOH}$  solution of Co@NC and commercial 20% Pt/C catalysts in (a) glassy carbon electrode (b) Ni foam. (c) the corresponding Tafel plots derived from data of (a). (d) LSVs recorded before and after 1250 cycles using the Co@NC/Ni foam catalyst.

HER activity of Co@NC catalyst deposited on Ni foam also showed similar results, in which the Pt/C catalyst outperformed the Co@NC catalyst, as shown in Figure 5c. The Co@NC catalyst showed an overpotential of 170 mV at  $10 \text{ mA}\cdot\text{cm}^{-2}$  current density, much higher than the Pt/C catalyst (2 mV); however, the HER activity of Co@NC catalyst was still appreciable due to the low cost of Co compared to Pt. The stability of the Co@NC catalyst was studied using the potential cycling process for 1250 cycles (Figure 5d). After 1250 potential cycles, the HER curves shifted negatively, with the overpotential being increased by 40 mV, at  $10 \text{ mA}\cdot\text{cm}^{-2}$  current density. These results indicate that the Co@NC catalyst under potential cycling conditions was still vulnerable to degradation. The degradation could be caused by various reasons such as carbon corrosion, leaching of Co nanoparticles or detachment of the catalyst from the Ni foam due to a weaker interaction between catalyst and Ni foam. The further HER Co@NC catalyst activity improvement could be realized by optimizing the synthesis conditions such as (i) increasing the loading of the precursor  $\text{Zn}_x\text{Co}_{1-x}(\text{C}_3\text{H}_4\text{N}_2)$  structures and hence the loading Co@NC catalyst, (ii) doping of a second heteroatom such as S or P, (iii) introducing second metal atom such as Fe, Se, Mn, etc., and (iv) optimizing the binder compositions. Despite the lower activity of the Co@NC catalyst, the obtained HER performance was still appreciable in terms of the lower cost of the Co-based catalyst when compared to the expensive Pt-based catalyst.

We further assessed the OER performance of Co@NC catalyst in  $1.0 \text{ M}$  aqueous KOH electrolyte and compared it with the commercially obtained  $\text{RuO}_2$  benchmark-catalyst activity. As shown in Figure 6a, the Co@NC catalyst showed a sudden increase in the current in the potential range of 1.4–1.6 V, signifying the considerable OER activity of the Co@NC catalyst. Both the catalysts reached a similar potential of 1.680 V (450 mV

overpotential) at a current density of  $10 \text{ mA} \cdot \text{cm}^{-2}$ . However, one could observe that the Co@NC catalyst showed positive OER onset potential compared to the benchmark  $\text{RuO}_2$ . These results indicate that the Co@NC catalyst was comparable to the  $\text{RuO}_2$  catalyst. Further, the Tafel slope of the Co@NC catalyst was also close to the  $\text{RuO}_2$  one, indicating that the Co@NC catalyst possessed comparable OER activity. We then tested the OER activity of the Co@NC catalyst deposited on Ni foam. For that, the in-situ generated Co@NC on Ni foam was tested by recording the LSV curve, which is shown in Figure 6b. For comparison, the LSV curves of bare Ni foam and  $\text{RuO}_2/\text{Ni}$  foam were recorded and are shown in Figure 6b. At the current density of 50 and  $100 \text{ mA} \cdot \text{cm}^{-2}$ , the overpotential of the Co@NC/Ni foam,  $\text{RuO}_2/\text{Ni}$  foam, and the bare Ni foam were 452, 585, 666 and 552, 694, and 784 mV, respectively. This indicated the high catalytic activity of the  $\text{RuO}_2/\text{Ni}$  foam towards OER. The LSV curve of the Co@NC/Ni foam showed an oxidation peak in the potential region of  $\sim 1.35\text{--}1.5 \text{ V}$ , which was ascribed to the surface oxidation of Co ( $\text{Co} \leftrightarrow \text{Co(II)} \leftrightarrow \text{Co(III)}$ ) [24–26].

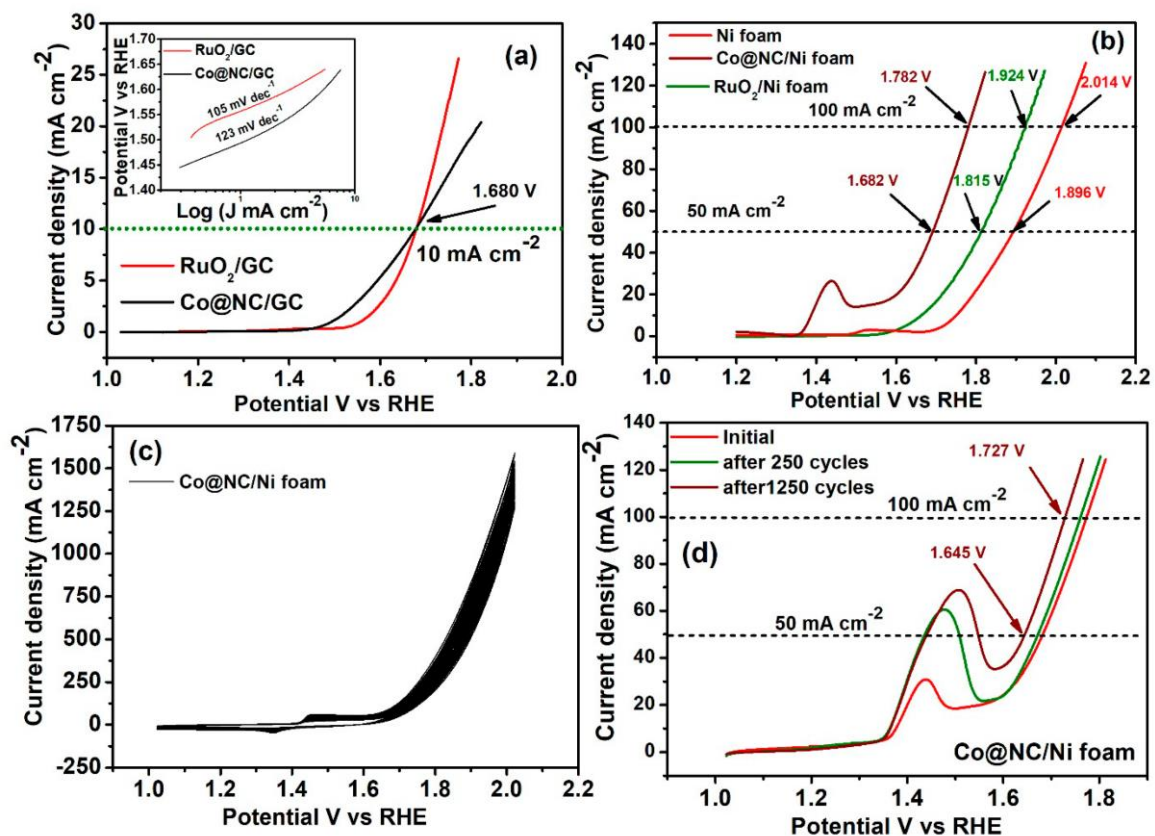


**Figure 6.** OER LSVs measured at  $5 \text{ mV} \cdot \text{s}^{-1}$  in  $1.0 \text{ M KOH}$  solution of Co@NC and commercial  $\text{RuO}_2$  catalysts in (a) glassy carbon electrode (b) Ni foam. the corresponding Tafel plots derived from data of (a) given in the inset of figure (a). (c) cyclic voltammograms of the Co@NC/Ni foam catalyst (d) LSVs recorded before and after 250 and 1250 cycles using Co@NC/Ni foam catalyst.

Strikingly, the OER activity of the Co@NC catalyst on Ni foam was found to be much higher than on the GC electrode. The significantly lower overpotential of the Co@NC/Ni foam compared to the  $\text{RuO}_2/\text{Ni}$  foam was due to the enhanced kinetics in the form of fast electron and ion/molecule transportation on the conductive Ni foam. Moreover, the generated gas ( $\text{H}_2/\text{O}_2$ ) bubbles on the Co@NC/Ni foam were immediately eliminated from the surface because of the microporosity of NC and the macroporosity of the Ni foam, which provided the active area for further oxygen evolution. The stability of the Co@NC/Ni foam catalyst was further evaluated by recording 1250 cyclic voltammogram curves continuously in the OER potential region (Figure 6c). In order to check the stability, the LSVs were

recorded after 250 and 1250 cycles and are shown in (Figure 6d. After 250 cycles, the catalytic activity was almost the same as that of the initial activity; however, after 1250 cycles, the potential at 50, and 100 mA cm<sup>-2</sup> current density shifted to a lower potential region (positive direction) with an overpotential gain of 37 and 55 mV, respectively. These results showed that the Co@NC/Ni foam has a relatively similar catalytic activity to that of RuO<sub>2</sub>, under similar experimental conditions and admirable stability towards OER. Generally, the alkaline electrochemical water splitting was hindered by the large overpotential of the anode electrode. Therefore, the low overpotential of the Co@NC/Ni foam electrode could significantly enhance overall water splitting.

Although a detailed understanding of the electrocatalytic activity of the Co@NC catalyst is indeed required, it was proposed in the literature that the electrocatalytic activity of the Co@NC catalyst might come from the structural and electronic interaction between the metal cores and the carbon shells [27,28]. Based on the literature results, we propose the following reasons being responsible for the superior electrocatalytic activity of the Co@NC catalyst towards HER and OER; (i) it has been well reported that the N doped carbon itself acts as a metal-free catalyst for electrocatalytic reactions, which include ORR, OER, and HER reactions, due to the presence of active graphitic-N and pyridinic-N sites [29]; (ii) the N-doped carbon shells increases the electronic conductivity of the Co@NC catalyst by fast transfer of electrons from the NC shells to the Co core nanoparticles and increased electronic density on the Co nanoparticles thus reduces the work function of Co nanoparticles towards the HER and OER reaction kinetics [30] (iii); the porous NC shell enhances the release of the product gases H<sub>2</sub> and O<sub>2</sub> from the Co@NC catalyst and also ensures the stability of the catalyst [31]. Based on the above reasons, it can be concluded that a prime factor responsible for the electrocatalytic activity of the Co@NC catalyst is the unique electronic interactions that arise between the metal cores and the carbon shells. And this interaction can be further tuned (i) by alloying the Co metal core with other transition metals and (ii) by synthesizing the catalyst with varying carbon layers (thickness of the carbon shells), and (iii) by doping the carbon shells with various heteroatoms with different electron-donating and withdrawing ability. Hence, there are still great opportunities for researchers that exist for tuning the electrocatalytic properties of the Co@NC catalyst for various electrochemical reactions. Table 1 shows the comparison of overall electrochemical water splitting performance of the Co@NC electrodes with those of various reported non-precious metal-based electrocatalysts [32–52]. After comparing from the literature values, the OER and HER activity of Co@NC catalyst was found to be better than other catalysts, and hence Co@NC could be a possible choice of catalyst for electrochemical water splitting applications.

**Table 1.** Comparison of HER and OER performance of Co@NC catalyst with reported non-precious transition metal-based electrocatalysts.

Catalyst	Electrolyte	Overpotential @10 mA·cm <sup>-2</sup> (mV)	Ref
<b>Hydrogen evolution reaction</b>			
Co <sub>2</sub> B/CoSe <sub>2</sub>	1 M KOH	300	[33]
Cubic CoSe <sub>2</sub> /GD	0.5 M H <sub>2</sub> SO <sub>4</sub>	200	[34]
Interwoven CoSe <sub>2</sub> /CNT	0.5 M H <sub>2</sub> SO <sub>4</sub>	186	[35]
CoSe <sub>2</sub> /CNT	0.5 M H <sub>2</sub> SO <sub>4</sub>	174	[36]
CoSe <sub>2</sub> hollow microsphere/rGo	0.5 M H <sub>2</sub> SO <sub>4</sub>	250	[37]
CoS/CC	1 M KOH	197	[38]
Co <sub>9</sub> S <sub>8</sub> /NC@MoS <sub>2</sub>	0.5 M H <sub>2</sub> SO <sub>4</sub>	217	[38]

Table 1. Cont.

Catalyst	Electrolyte	Overpotential @10 mA·cm <sup>-2</sup> (mV)	Ref
Co@BCN	1.M KOH	183	[39]
Co-NCNTs-10	1.M KOH	204	[40]
N-Co@G	0.1 M NaOH	337	[41]
Co <sub>0.75</sub> Fe <sub>0.25</sub> -NC	1.0 M KOH	202	[42]
G-Coated Cu NWs	0.5 M H <sub>2</sub> SO <sub>4</sub>	252	[43]
FeCo@N-C	0.5 M H <sub>2</sub> SO <sub>4</sub>	230	[44]
Ni@graphene	1.0 M KOH	240	[45]
Co@NC/GC	1.0 M KOH	243 @ 10 mA cm <sup>-2</sup>	This work
Co@NC/Ni	1.0 M KOH	170 @ 10 mA cm <sup>-2</sup>	This work
Oxygen Evolution Reaction			
Fe/N-CNTs	1.0 M KOH	520	[46]
Ni/N-CNTs	1.0 M KOH	590	[46]
NiCo <sub>2</sub> O <sub>4</sub>	1.0 M KOH	490	[47]
CuCo <sub>2</sub> O <sub>4</sub> /NrGO	1.0 M PBS	1150	[48]
MnFe <sub>2</sub> O <sub>4</sub>	1.0 M KOH	470	[49]
Ni Fe <sub>2</sub> O <sub>4</sub>	1.0 M KOH	440	[49]
Ni <sub>3</sub> N bulk	1.0 M KOH	490	[50]
FeOOH	1.0 M KOH	533	[51]
IrO <sub>2</sub>	1.0 M KOH	587	[52]
Co@NC/GC	1.0 M KOH	450 @ 10 mA cm <sup>-2</sup>	This work
Co@NC/Ni	1.0 M KOH	452 @ 50 mA cm <sup>-2</sup>	This work

#### 4. Conclusions

In summary, we developed a simple, cost-efficient strategy to synthesis well-defined Co@NC core-shell nanostructures by a simple mechano-chemical synthesis process. TEM analysis showed a Co@NC nanoparticle of an average ~10–12 nm size was obtained by the synthesis process. TEM analysis showed Co@NC core-shell nanoparticles and even the distribution on the N-doped carbon support. Electrochemical characterization of the catalysts showed that Co@NC nanoparticles showed an enhanced OER activity, with excellent stability for 1250 cycles. In addition, the Co@NC catalyst also showed decent HER activity; however, under the HER region, the Co@NC catalyst showed a slightly degraded characteristic. These results indicate that the Co@NC catalyst could be a good choice for OER reactions in various electrochemical energy devices.

**Author Contributions:** Conceptualization and methodology, S.G.P.; Resources, R.K.; validation, C.L.; writing—original draft, S.G.P.; editing, G.R. and A.A.; resources, C.V.R.; funding acquisition, S.G.P. All authors have read and agreed to the published version of the manuscript.

**Funding:** This research work was supported by Keimyung University, Research Grant No. 20190678.

**Institutional Review Board Statement:** Not applicable.

**Informed Consent Statement:** Not applicable.

**Data Availability Statement:** Not applicable.

**Acknowledgments:** This research work was supported by Keimyung University, Research Grant No. 20190678. The author S.G.P. also thanks C.V.R. A.A. and G.R. for helping in physical and electrochemical characterizations of the catalysts.

**Conflicts of Interest:** The authors declare that they have no known competing financial interests or personal relationships that could have appeared to influence the work reported in this paper.

## References

1. Wang, L.; Li, Y.; Xia, M.; Li, Z.; Chen, Z.; Ma, Z.; Qina, X.; Shao, G. Ni nanoparticles supported on graphene layers: An excellent 3D electrode for hydrogen evolution reaction in alkaline solution. *J. Power Sources* **2017**, *347*, 220–228. [CrossRef]
2. Tian, B.; Zhen, W.; Gao, H.; Zhang, X.; Li, Z.; Lu, G. Carboxyl-assisted synthesis of Co nanorods with high energy facet on graphene oxide sheets for efficient photocatalytic hydrogen evolution. *Appl. Catal. B Environ.* **2017**, *203*, 789–797. [CrossRef]
3. Wang, L.; Li, Y.; Yin, X.; Wang, Y.; Lu, L.; Song, A.; Xia, M.; Li, Z.; Qin, X.; Shao, G. Comparison of three nickel-based carbon composite catalysts for hydrogen evolution reaction in alkaline solution. *Int. J. Hyd. Energy* **2017**, *42*, 22655–22662. [CrossRef]
4. Reddy, S.; Song, L.; Kang, L.; Feng, Q.; Du, R.; Zhang, J.; He, L.; Seeram, R. Preparation of Mo<sub>2</sub>C–carbon nanomaterials for hydrogen evolution reaction. *Carbon Lett.* **2019**, *29*, 225–232. [CrossRef]
5. Zhao, L.; Mingming, L.; Mingwei, C.; Xiaopeng, Q.; Juan, L.; Chao, L.; Peera, S.G.; Tongxiang, L. Exploring the oxygen electrode bi-functional activity of Ni–N–C-doped graphene systems with N, C co-ordination and OH ligand effects. *J. Mater. Chem. A* **2020**, *8*, 20453–20462.
6. Haihong, Z.; Carlos, A.C.R.; Yuan, Z.; Shuwei, Z.; Yongjun, F.; Nicolas, A.V. Recent Advances of Cobalt-Based Electrocatalysts for Oxygen Electrode Reactions and Hydrogen Evolution Reaction. *Catalysts* **2018**, *8*, 559.
7. Jamesh, M.I.; Sun, X. Recent progress on earth abundant electrocatalysts for oxygen evolution reaction (OER) in alkaline medium to achieve efficient water splitting—a review. *J. Power Sources* **2018**, *400*, 31–68. [CrossRef]
8. Ziliang, C.; Huilin, Q.; Kun, Z.; Dalin, S.; Renbing, W. Metal-organic framework-derived nanocomposites for electrocatalytic hydrogen evolution reaction. *Prog. Mat. Sci.* **2020**, *108*, 100618.
9. Ya, Y.; Bao, Y.X.; Bin, Z.; Xin, W.A. review on noble-metal-free bifunctional heterogeneous catalysts for overall electrochemical water splitting. *J. Mater. Chem. A* **2016**, *4*, 17587–17603.
10. Hele, G.; Qichun, F.; Jixin, Z.; Jingsan, X.; Qianqian, L.; Siliang, L.; Kaiwen, X.; Chao, Z.; Tianxi, L. Cobalt nanoparticle-embedded nitrogen-doped carbon/carbon nanotube frameworks derived from a metal–organic framework for tri-functional ORR, OER and HER electrocatalysis. *J. Mater. Chem. A* **2019**, *7*, 3664–3672.
11. Hao-Fan, W.; Liyu, C.; Huan, P.; Stefan, K.; Qiang, X. MOF-derived electrocatalysts for oxygen reduction, oxygen evolution and hydrogen evolution reactions. *Chem Soc. Rev.* **2020**, *49*, 1414–1448.
12. Shaik, G.P.; Kwon, H.J.; Lee, T.G. Highly efficient Co@NCS nanosheet electrocatalyst for oxygen reduction reaction: An environment-friendly, low-cost and sustainable electrocatalyst. *Mater. Res. Bull.* **2020**, *128*, 110873. [CrossRef]
13. Remya, V.R.; Kurian, M. Synthesis and catalytic applications of metal–organic frameworks: A review on recent literature. *Int. Nano Lett.* **2019**, *9*, 17–29. [CrossRef]
14. Available online: [www.chemistryworld.com/news/enhancing-solvents-sustainability/3010810.article](http://www.chemistryworld.com/news/enhancing-solvents-sustainability/3010810.article) (accessed on 7 August 2019).
15. Peera, S.G.; Jayaraman, B.; Nam, H.K.; Joong, H.L. Sustainable Synthesis of Co@NC Core Shell Nanostructures from Metal Organic Frameworks via Mechanochemical Coordination Self-Assembly: An Efficient Electrocatalyst for Oxygen Reduction Reaction. *Small* **2018**, *14*, 1800441–1800456. [CrossRef]
16. Bo, Y.; Nan, J.; Meili, S.; Walter, S.D.; Junko, Y.; Yujie, S. Bimetal–Organic Framework Self-Adjusted Synthesis of Support-Free Nonprecious Electrocatalysts for Efficient Oxygen Reduction. *ACS Catal.* **2015**, *5*, 7068–7076.
17. Peera, S.G.; Kwon, H.J.; Lee, T.G.; Hussain, A.M. Heteroatom- and metalloid-doped carbon catalysts for oxygen reduction reaction: A mini-review. *Ionics* **2020**, *26*, 1563–1589. [CrossRef]
18. Yunhe, S.; Hongliang, J.; Yihua, Z.; Xiaoling, Y.; Jianhua, S.; Wenjian, Z.; Jianding, C.; Chunzhong, L. Enriched graphitic N-doped carbon-supported Fe<sub>3</sub>O<sub>4</sub> nanoparticles as efficient electrocatalysts for oxygen reduction reaction. *J. Mater. Chem. A* **2014**, *2*, 7281–7287.
19. Wenxiu, Y.; Xiangjian, L.; Xiaoyu, Y.; Jianbo, J.; Shaojun, G. Bamboo-like Carbon Nanotube/Fe<sub>3</sub>C Nanoparticle Hybrids and Their Highly Efficient Catalysis for Oxygen Reduction. *J. Am. Chem. Soc.* **2015**, *137*, 1436–1439.
20. Yuke, S.; Wenfu, X.; Shijin, L.; Jian, G.; Mingfei, S. Hierarchical Hollow Co/N–C@NiCo<sub>2</sub>O<sub>4</sub> Microsphere as an Efficient Bi-functional Electrocatalyst for Rechargeable Zn–Air Battery. *Front. Mater.* **2019**, *6*, 261.
21. Peng, Y.; Lei, W.; Fanfei, S.; Ying, X.; Xu, L.; Jingyuan, M.; Xiwen, W.; Chungui, T.; Jinghong, L.; Honggang, F. Co Nanoislands Rooted on Co–N–C Nanosheets as Efficient Oxygen Electrocatalyst for Zn–Air Batteries. *Adv. Mater.* **2019**, *31*, 1901666–1901675.
22. Xiaojing, Z.; Jiale, D.; Ligui, L.; Zexing, W.; Shaowei, C. N, S co-doped hierarchical porous carbon spheres embedded with cobalt nanoparticles as efficient bifunctional oxygen electrocatalysts for rechargeable zinc-air batteries. *Nanoscale* **2019**, *11*, 21302–21310.
23. Lu, J.; Yin, S.; Shen, P.K. Carbon-Encapsulated Electrocatalysts for the Hydrogen Evolution Reaction. *Electrochem. Energ. Rev.* **2019**, *2*, 105–127. [CrossRef]
24. Bangan, L.; Dianxue, C.; Pan, W.; Guiling, W.; Yinyi, G. Oxygen evolution reaction on Ni-substituted Co<sub>3</sub>O<sub>4</sub> nanowire array electrodes. *Int. J. Hyd. Energy* **2011**, *36*, 72–78.

25. Gang, W.; Ning, L.; De-Rui, Z.; Kurachi, M.; Bo-Qing, X. Anodically electrodeposited CoNi mixed oxide electrode: Preparation and electrocatalytic activity for oxygen evolution in alkaline media. *J. Solid State Chem.* **2004**, *177*, 3682–3692.
26. Rajeshkhanna, G.; Umeshbabu, E.; Rao, G.R. In situ grown nano-architectures of Co<sub>3</sub>O<sub>4</sub> on Ni-foam for charge storage application. *J. Chem. Sci.* **2017**, *129*, 157–166. [[CrossRef](#)]
27. Yang, H.; Jens, O.J.; Wei, Z.; Lars, N.C.; Wei, X.; Niels, J.B.; Qingfeng, L. Hollow Spheres of Iron Carbide Nanoparticles Encased in Graphite Layers as Oxygen Reduction Catalysts. *Angew. Chem. Int. Ed.* **2014**, *53*, 3675–3679.
28. Jiao, D.; Liang, Y.; Dehui, D.; Xiaoqi, C.; Fan, Y.; Xinhe, B. Highly active reduction of oxygen on a FeCo alloy catalyst encapsulated in pod-like carbon nanotubes with fewer walls. *J. Mater. Chem. A* **2013**, *1*, 14868–14873.
29. Zheng, Y.; Jiao, Y.; Zhu, Y.; Li, L.H.; Han, Y.; Chen, Y.; Du, A.; Jaroniec, M.; Qiao, S.Z. Hydrogen evolution by a metal-free electrocatalyst. *Nat. Commun.* **2014**, *5*, 3783. [[CrossRef](#)] [[PubMed](#)]
30. Xiaoxin, Z.; Xiaoxi, H.; Anandarup, G.; Rafael, S.; Bhaskar, R.S.; Eliška, M.; Tewodros, A. Cobalt-embedded nitrogen-rich carbon nanotubes efficiently catalyze hydrogen evolution reaction at all pH values. *Angew. Chem. Int. Ed.* **2014**, *53*, 4372–4376.
31. Bo, Y.; Nan, J.; Meili, S.; Sheraz, G.; Junko, Y.; Yujie, S. High-Performance Overall Water Splitting Electrocatalysts Derived from Cobalt-Based Metal–Organic Frameworks. *Chem. Mater.* **2015**, *27*, 7636–7642.
32. Nannan, Y.; Qianqian, J.; Jie, L.; Jianguo, T. A review on non-noble metal based electrocatalysis for the oxygen evolution reaction. *Arab. J. Chem.* **2020**, *13*, 4294–4309.
33. Yaxiao, G.; Zhaoyang, Y.; Changshuai, S.; Erkang, W. Amorphous Co<sub>2</sub>B Grown on CoSe<sub>2</sub> Nanosheets as a Hybrid Catalyst for Efficient Overall Water Splitting in Alkaline Medium. *ACS Appl. Mater. Interfaces* **2017**, *9*, 39312–39317.
34. Hongxiu, Z.; Lecheng, L.; Xingwang, Z. One-Step Synthesis of Cubic Pyrite-Type CoSe<sub>2</sub> at Low Temperature for Efficient Hydrogen Evolution Reaction. *RSC Adv.* **2014**, *4*, 54344–54348.
35. Yue, H.H.; Yu, B.; Qi, F.; Zhou, J.H.; Wang, X.Q.; Zheng, B.J.; Zhang, W.L.; Li, Y.R.; Chen, Y.F. Interwoven CoSe<sub>2</sub>/CNTs Hybrid as a Highly Efficient and Stable Electrocatalyst for Hydrogen Evolution Reaction. *Electrochim. Acta* **2017**, *253*, 200–207. [[CrossRef](#)]
36. Kim, J.K.; Park, G.D.; Kim, J.H.; Park, S.K.; Kang, Y.C. Rational Design and Synthesis of Extremely Efficient Macroporous CoSe<sub>2</sub>-CNT Composite Microspheres for Hydrogen Evolution Reaction. *Small* **2017**, *13*, 1700068. [[CrossRef](#)]
37. Dai, C.; Tian, X.K.; Nie, Y.L.; Tian, C.; Yang, C.; Zhou, Z.X.; Li, Y.; Gao, X.Y. Successful Synthesis of 3D CoSe<sub>2</sub> Hollow Microspheres with High Surface Roughness and its Excellent Performance in Catalytic Hydrogen Evolution Reaction. *Chem. Eng. J.* **2017**, *321*, 105–112. [[CrossRef](#)]
38. Li, N.; Liu, X.; Li, G.D.; Wu, Y.Y.; Gao, R.Q.; Zou, X.X. Vertically Grown CoS Nanosheets on Carbon Cloth as Efficient Hydrogen Evolution Electrocatalysts. *Int. J. Hydrogen Energy* **2017**, *42*, 9914–9921. [[CrossRef](#)]
39. Zhang, H.B.; Ma, Z.J.; Duan, J.; Huimin, L.; Guigao, L.; Tao, W.; Kun, C.; Mu, L.; Li, S.; Xianguang, M.; et al. Active sites implanted carbon cages in core shell architecture: Highly active and durable electrocatalyst for hydrogen evolution reaction. *ACS Nano* **2016**, *10*, 684–694. [[CrossRef](#)] [[PubMed](#)]
40. Zhang, S.Y.; Xiao, X.X.; Lv, T.T.; Xiaomeng, L.; Botao, L.; Wei, W.; Liu, J. Cobalt encapsulated N-doped defect-rich carbon nanotube as pH universal hydrogen evolution electrocatalyst. *Appl. Surf. Sci.* **2018**, *446*, 10–17. [[CrossRef](#)]
41. Fei, H.; Yang, Y.; Peng, Z.W.; Gedeng, R.; Qifeng, Z.; Lei, L.; Errol, L.G.S.; James, M.T. Cobalt nanoparticles embedded in nitrogen-doped carbon for the hydrogen evolution reaction. *ACS Appl. Mater. Interfaces* **2015**, *7*, 8083–8087. [[CrossRef](#)]
42. Feng, X.G.; Bo, X.J.; Guo, L.P. CoM(M = Fe, Cu, Ni)-embedded nitrogen-enriched porous carbon framework for efficient oxygen and hydrogen evolution reactions. *J. Power Sources* **2018**, *389*, 249–259. [[CrossRef](#)]
43. Manikandan, A.; Lee, L.; Wang, Y.C.; Chen, C.W.; Chen, Y.Z.; Henry, M.; Tseng, J.Y.; Zhiming, M.W.; Chueh, Y.L. Graphene-coated copper nanowire networks as a highly stable transparent electrode in harsh environments toward efficient electrocatalytic hydrogen evolution reactions. *J. Mater. Chem. A* **2017**, *5*, 13320–13328. [[CrossRef](#)]
44. Noh, S.H.; Seo, M.H.; Kang, J.; Takeyoshi, O.; Byungchan, H.; Takeo, O. Towards a comprehensive understanding of FeCo coated with N-doped carbon as a stable bi-functional catalyst in acidic media. *NPG Asia Mater.* **2016**, *8*, e312. [[CrossRef](#)]
45. Ai, L.H.; Tian, T.; Jiang, J. Ultrathin graphene layers encapsulating nickel nanoparticles derived metal-organic frameworks for highly efficient electrocatalytic hydrogen and oxygen evolution reactions. *ACS Sustain. Chem. Eng.* **2017**, *5*, 4771–4777. [[CrossRef](#)]
46. Yanyan, L.; Hongliang, J.; Yihua, Z.; Xiaoling, Y.; Chunzhong, L. Transition metals (Fe, Co, and Ni) encapsulated in nitrogen-doped carbon nanotubes as bi-functional catalysts for oxygen electrode reactions. *J. Mater. Chem. A* **2016**, *4*, 1694–1701.
47. Dong, U.L.; Bae, J.K.; Zhongwei, C. One-pot synthesis of a mesoporous NiCo<sub>2</sub>O<sub>4</sub> nanoplatelet and graphene hybrid and its oxygen reduction and evolution activities as an efficient bi-functional electrocatalyst. *J. Mater. Chem. A* **2013**, *1*, 4754–4762.
48. Santosh, K.B.; Pagona, P. CuCo<sub>2</sub>O<sub>4</sub> nanoparticles on nitrogenated graphene as highly efficient oxygen evolution catalyst. *J. Power Sources* **2015**, *281*, 243–251.
49. Mian, L.; Yueping, X.; Xiaotian, L.; Xiangjie, B.; Yufan, Z.; Ce, H.; Liping, G. Facile synthesis of electrospun MFe<sub>2</sub>O<sub>4</sub> (M = Co, Ni, Cu, Mn) spinel nanofibers with excellent electrocatalytic properties for oxygen evolution and hydrogen peroxide reduction. *Nanoscale* **2015**, *7*, 8920–8930.
50. Kun, X.; Pengzuo, C.; Xiuling, L.; Yun, T.; Hui, D.; Xiaojun, W.; Wangsheng, C.; Zhenmeng, P.; Changzheng, W.; Yi, X. Metallic Nickel Nitride Nanosheets Realizing Enhanced Electrochemical Water Oxidation. *J. Am. Chem. Soc.* **2015**, *137*, 4119–4125.

- 
51. Swierk, J.R.; Klaus, S.; Trotochaud, L.; Bell, A.T.; Tilley, T.D. Electrochemical Study of the Energetics of the Oxygen Evolution Reaction at Nickel Iron (Oxy)Hydroxide Catalysts. *J. Phys. Chem. C* **2015**, *119*, 19022–19029. [[CrossRef](#)]
  52. Li, F.; Bu, Y.; Lv, Z.; Mahmood, J.; Han, G.-F.; Ahmad, I.; Kim, G.; Zhong, Q.; Baek, J.-B. Porous Cobalt Phosphide Polyhedrons with Iron Doping as an Efficient Bifunctional Electrocatalyst. *Small* **2017**, *13*, 1701167. [[CrossRef](#)] [[PubMed](#)]